Phonon control of magnetic relaxation in the pyrochlore slab compounds $SrCr_{9x}Ga_{12-9x}O_{19}$ and $Ba_2Sn_2ZnCr_{7x}Ga_{10-7x}O_{22}$

Mohamed Zbiri,* Hannu Mutka, Mark R. Johnson, and Helmut Schober
Institut Max von Laue-Paul Langevin, 6 rue Jules Horowitz, BP 156, 38042 Grenoble Cedex 9, France

Christophe Payen
Institut des Matériaux Jean Rouxel, Université de Nantes–CNRS, BP 32229, 44322 Nantes Cedex 3, France
(Received 18 December 2009; revised manuscript received 26 February 2010; published 17 March 2010)

We are interested in the phonon response in the frustrated magnets $SrCr_{9x}Ga_{12-9x}O_{19}$ (SCGO) and $Ba_2Sn_2ZnCr_{7x}Ga_{10-7x}O_{22}$ (BSZCGO). The motivation of the study is the recently discovered, phonon-driven, magnetic relaxation in the SCGO compound [Mutka *et al.*, Phys. Rev. Lett. **97**, 047203 (2006)] pointing out the importance of a low-energy ($\hbar\omega \sim 7$ meV) phonon mode. In neutron-scattering experiments on these compounds, the phonon signal is partly masked by the magnetic signal from the Cr moments and we have therefore examined in detail the nonmagnetic isostructural counterparts $SrGa_{12}O_{19}$ (SGO) and $Ba_2Sn_2ZnGa_{10}O_{22}$ (BSZGO). Our *ab initio* lattice-dynamics calculations on SGO reveal a peak in the vibrational density of states matching with the neutron observations on SGO and SCGO. A strong contribution in the vibrational density of states comes from the partial contribution of the Ga atoms on the 2*b* and 12*k* sites, involving modes at the M point of the hexagonal system. These modes comprise dynamics of the Kagomé planes of the pyrochlore slab magnetic sublattice, 12*k* sites, and therefore can drive magnetic relaxation via spin-phonon coupling. Both BSZCGO and BSZGO show a similar low-energy Raman peak but no corresponding peak in the neutron-determined density of states of BSZGO is seen. However, a strong non-Debye enhancement of low-energy phonon response is observed. We attribute this particular feature to the Zn/Ga disorder on the 2*d* site, already evoked earlier to affect the magnetic properties of BSZCGO. We propose that this disorder-induced phonon response explains the absence of a characteristic energy scale and the much faster magnetic relaxation observed in BSZCGO.

DOI: 10.1103/PhysRevB.81.104414 PACS number(s): 75.50.Lk, 63.20.dk, 78.70.Nx, 71.15.Mb

I. INTRODUCTION

The interplay between structural, electronic, and dynamic degrees of freedom in geometrically frustrated magnetic materials has the consequence of creating highly degenerate ground states, which have generated considerable interest.[1–3] Short-range correlations in frustrated magnets lead to the formation of weakly coupled, fluctuating clusters and consequently a macroscopic, collective degeneracy can prevail.[1,4–6]

At low temperature, frustrated magnets are expected to be sensitive to weak perturbations, which can raise the ground-state degeneracy, produce a hierarchy of closely space energy levels and allow the possibility of slow dynamics at low temperature between the corresponding states. When the associated energy scales of these states fall well below that of magnetic interactions,[4,7] various perturbations including static[8] or dynamic[9,10] lattice effects may play a key role due to coupling between lattice and magnetic degrees of freedom. A recent neutron spin-echo (NSE) examination of the pyrochlore slab antiferromagnet (Kagome bilayer) $SrCr_{9x}Ga_{12-9x}O_{19}$ (SCGO) (Ref. 11) suggested that phonons affect the slow relaxation of this highly frustrated spin system. The SCGO compound has a particular ground state in which dimer correlations within the pyrochlore slabs show a partial freezing of about 1/3 of the total possible ordered magnetic moment in spite of the high value of the average intraslab superexchange interaction ($\sim$13 meV).[12] The frozen ground state does not fit into a spin-glass picture, for example, it has been shown that both the freezing transition temperature and the frozen moment decrease with increased level of magnetic dilution due to the Ga/Cr substitution.[13]

The extremely broad relaxation seen using NSE spectroscopy was fitted with a phenomenological stretched exponential time dependence to infer an activated temperature dependence with an activation energy of $E_a \sim 7$ meV.[11] A vibrational mode was observed close to this same position by Raman spectroscopy and inelastic neutron scattering (INS), leading to the conclusion that phonons drive the relaxation. However, why phonons at 7 meV, and not other frequencies, drive magnetic relaxation is not clear and further investigation of phonons and related spin-phonon mechanisms is required. In this context, we have studied the isostructural nonmagnetic material $SrGa_{12}O_{19}$ (SGO) using *ab initio* lattice-dynamics calculations that provide a full picture of the phonon-dispersion relations, total and partial density of states, energies of Raman-active modes, and the neutron-scattering cross section. The choice of the nonmagnetic counterpart SGO is motivated by experimental considerations (see below) and the fact that, practically, handling the chemical disorder associated with the Cr/Ga substitution in SCGO efficiently is not feasible in the lattice-dynamics calculation. The calculated neutron-scattering cross section is used for the evaluation of the powder-averaged Q-dependent intensity that can be compared with experiment. The calculations are accompanied by new experiments using INS and Raman spectroscopy. Experimental techniques are combined because Raman spectroscopy gives a partial view of the vi-

brational density of states (Γ point only) which is complemented by INS that can inform on the Q dependence and characteristic energies throughout the Brillouin zone.

In addition to the SCGO/SGO case, we have examined the experimental situation in the related pyrochlore slab compound $Ba_2Sn_2ZnCr_{7x}Ga_{10-7x}O_{22}$ (BSZCGO) and its nonmagnetic counterpart $Ba_2Sn_2ZnGa_{10}O_{22}$ (BSZGO). *Ab initio* lattice-dynamics calculations could not be done for BSZCGO and BSZGO due to their complex crystal structures. In BSZCGO, the magnetic relaxation rate at low T was observed to be by some two orders of magnitude faster than in SCGO but without a well-defined energy scale.[11] Nevertheless, both in BSZCGO and BSZGO, Raman data reveal a phonon peak at an energy close to the one seen in SCGO and SGO while no peak is seen in the INS response. As we shall see below, the absence of a characteristic energy in the relaxation of BSZCGO makes more sense when we consider the rather strong non-Debye enhancement of the phonon DOS that we attribute to the substitutional disorder, the 50/50 mix of Zn and Ga on the 2d site in this compound.[14] Accordingly, we conclude that the localized phonon modes associated with the substitutional disorder can also affect the magnetic interactions and induce relaxational dynamics of the magnetic system. These observations also point out the particularity of the frustrated magnets concerning the system dependence of the low-energy properties.

As for SCGO, the aim of the present work is (i) to identify from *ab initio* calculations the experimentally observed phonon modes (neutron and Raman spectroscopy), these calculations were used to obtain generalized neutron-weighted vibrational density of states (GDOS) and the active Raman modes for SGO, (ii) understand the importance of non-Γ-point modes, and (iii) investigate the normal modes having an effect on the dynamics of the magnetic sites and hence the possibility to drive magnetic relaxation.

This paper is organized as follows. The experimental and computational details are provided in Secs. II and III, respectively. Section IV is dedicated to the presentation of the results that are discussed in Sec. V with conclusions.

II. EXPERIMENTAL DETAILS

Powder samples of nonmagnetic SGO and BSZGO were prepared using a standard solid-state high-temperature ceramic synthesis method and characterized by x-ray and neutron diffraction. As for the magnetic SCGO ($x=0.95$) and BSZCGO ($x=0.97$) samples, we analyzed those that were already used in our previous studies.[11,13–15] The INS measurements were performed at the Institut Laue Langevin (ILL) (Ref. 16) (Grenoble, France), using two instruments; the cold neutron time-of-flight spectrometer IN6 and the thermal-neutron time-of-flight spectrometer IN4. IN6 operating with an incident wavelength of $\lambda_i=4.1$ Å provides very good resolution [0.2 meV full width at half maximum (FWHM)] in the lower energy-transfer range ($|\hbar\omega| \leq 10$ meV) for the anti-Stokes spectrum. On IN4 using incident wavelengths of $\lambda_i=2.6$ or 1.8 Å, one has an extended Q range and this allows the Stokes spectrum to be measured at low temperature over a broader energy-transfer range with a resolution of 0.5 meV or 1 meV (FWHM), respectively. Experiments were performed on both SCGO/SGO and BSZCGO/BSZGO systems mainly at $T=300$ K and also at low temperatures $2<T<12$ K for SCGO/SGO. The data analysis was done using ILL software tools and the GDOS was evaluated using standard procedures[17] without applying multiphonon corrections. The experimental GDOS was normalized to $3N$ modes, where N is the number of atoms in the formula unit. Raman measurements at $T=300$ K were performed at the Institut des Matériaux Jean Rouxel (IMN).[18]

III. COMPUTATIONAL DETAILS

Relaxed geometries and total energies were obtained using the projector-augmented wave formalism[19] of the Kohn-Sham formulation of the density-functional theory[20,21] at the generalized gradient approximation (GGA) level, implemented in the Vienna *ab initio* simulation package (VASP).[22,23] The GGA was formulated by the Perdew-Burke-Ernzerhof[24,25] density functional. All results are well converged with respect to k mesh and energy cutoff for the plane-wave expansion. The break conditions for the self-consistent field and for the ionic relaxation loops were set to 10^{-6} eV Å^{-1} and 10^{-4} eV Å^{-1}, respectively. Hellmann-Feynman forces following geometry optimization were less than 10^{-4} eV Å^{-1}. Full geometry optimization, including cell parameters, was carried out on the experimentally refined SGO structure[26] containing 11 crystallographically inequivalent atoms (5 O, 5 Ga, and 1 Sr). A comparison of the *ab initio* optimized and experimental structural parameters is given in the Table I. The space group is $P6_3/mmc$ with 2 f.u. per unit cell (64 atoms). In order to determine all force constants, the supercell approach was used for lattice-dynamics calculations. An orthorhombic supercell was constructed from the relaxed structure containing 8 f.u. (256 atoms). A second partial geometry optimization (fixed lattice parameters) was performed on the supercell in order to further minimize the residual forces. Total energies and Hellmann-Feynman forces were calculated for 90 structures resulting from individual displacements of the symmetry inequivalent atoms in the supercell, along the inequivalent cartesian directions ($\pm x$, $\pm y$, and $\pm z$). 192 phonon branches corresponding to the 64 atoms in the primitive cell, were extracted from subsequent calculations using the direct method[28] as implemented in the PHONON software.[29] The coherent dynamic structure factor $S(Q,\omega)$ was calculated by the numerical procedure for evaluation of powder-averaged lattice dynamics.[30,31] For a list of wave vectors K with randomly chosen directions, but lengths corresponding to the Q range of interest, the dynamical matrix is diagonalized for each wave vector and the corresponding eigenfrequencies and eigenvectors are used to calculated $S(Q,\omega)$ for one-phonon creation. The wave vectors, spectral frequencies, and intensities are then used to construct the two-dimensional $S(Q,\omega)$ map, which can be compared with the measured map as will be shown below.

IV. RESULTS

A. SGO/SCGO phonon response from experiments

Figure 1 shows the $S(Q,\omega)$ intensity maps measured at $T=300$ K using the IN4 spectrometer, for both the magnetic

TABLE I. Lattice parameters and the relevant Ga/Cr position parameters from *ab initio* calculations on SGO compared with experimental data on SGO and SCGO.

		SGO (expt.) (Ref. 26)			SCGO (expt.) (Ref. 27)
Parameter	SGO (calc.)	$T=473$ K	$T=298$ K	$T=16$ K	$T=4.2$ K
a (Å)	5.86	5.80	5.80	5.79	5.80
c (Å)	22.87	22.86	22.82	22.78	22.66
$2a:x,y,z$	0, 0, 0	0, 0, 0	0, 0, 0	0, 0, 0	0, 0, 0[b]
$2b(4e):x,y,z$ [a,c]	0, 0, 1/4	0, 0, 1/4(0.258)	0, 0, 1/4(0.257)	0, 0, 1/4 (0.256)	0, 0, 1/4(0.256)
$12k:x,z$	0.1678, 0.891	0.1684, 0.891	0.1683, 0.891	0.1682, 0.891	0.1681, 0.892[b]
$4f_{iv}:z$ [c]	0.0278	0.0273	0.0273	0.0274	0.0283
$4f_{vi}:z$	0.190	0.190	0.190	0.190	0.192[b]

[a]For refinement of experimental data it is possible to split the $2b$ occupation over two $4e$ sites (Refs. 26 and 27).

[b]Cr occupation $\gtrsim$90% in least diluted samples (Ref. 13). The Kagome ($12k$) and triangular ($2a$) planes form the pyrochlore slab.

[c]Ga occupation 100%.

system SCGO and its nonmagnetic counterpart SGO. The strong intensity at low Q centered in the elastic position in SCGO is due to the quasielastic magnetic response resulting from the fluctuating $S=3/2$ moments of the Cr^{3+} atoms. Note that the Q dependence of the magnetic response is modulated with a main maximum at $Q=1.4$ Å^{-1} and the paramagnetic form factor gives just an overall trend. In spite of the decay of the magnetic form factor with increasing Q, this signal dominates and swamps the phonon signal. The $S(Q,\omega)$ map of SGO shows the phonon signal clearly visible in the absence of the magnetic response and it is possible to correlate

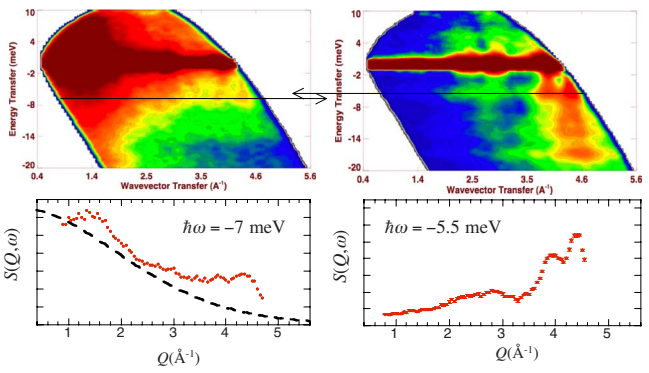

FIG. 1. (Color online) Measured $S(Q,\omega)$ maps at $T=300$ K for SCGO (top left) and SGO (top right). Strong paramagnetic scattering dominates the low-Q response of SCGO. We can note that a peaked phonon response comparable to the one seen in SGO at $\hbar\omega\approx-5.5$ meV with Q-dependent intensity is observed in SCGO at the highest Q range but at a slightly shifted energy transfer $\hbar\omega\approx-7$ meV, as shown by the arrows. The bottom panels show the constant energy-transfer scans at $\hbar\omega=-7$ meV for SCGO (bottom left) and at $\hbar\omega=-5.5$ meV for SGO (bottom right). For SCGO, the magnetic form factor Q dependence is shown (dashed line) in order to indicate the trend of the magnetic scattering. The phonons in SCGO appear less structured and somewhat blurred due to the weaker coherent scattering power of Cr atoms as well as due to the overlap with the magnetic signal.

the 7 meV features at highest Q range, $Q\geq3.5$ Å^{-1}, in SCGO with the 5.5 meV features in nonmagnetic sample SGO. As we can see phonons in SCGO are masked due to the presence of the magnetic signal and therefore are difficult to measure. In addition, the chemical disorder arising from the Cr substitution on the Ga sites, which can, in principle, be modeled, leads, in practice, to phonon instabilities in the calculations. For these reasons, this study is focused on the nonmagnetic material SGO. These results are then used with proper care to explain phonon-related phenomena in the magnetic system SCGO. The two systems are isostructural and accordingly the magnetic Cr sublattice sites can be identified crystallographically using the corresponding positions of the Ga atoms. Even though it is clear that the phonon response of the two systems cannot be identical both Raman spectroscopy and INS provide justification for our approach since the spectra of SCGO and SGO display similar features in the low-lying frequency range. This is reported in Fig. 2 for the Raman data. Both samples show a low-energy mode at ~53 cm^{-1} (~6.6 meV) and at ~60 cm^{-1} (~7.4 meV) for SGO and SCGO, respectively. Also the measured neutron density of states of the two systems follow quite similar trends, see Fig. 3. No attempt was made to eliminate the magnetic contribution that, in spite of being small, influences the GDOS evaluated for SCGO in the low-energy range. Supposing that the low-energy Raman mode is characteristic of Ga/Cr vibrations, we can argue that the shift of positions of the main low-frequency features is partly connected to the different masses of Cr and Ga atoms, 52 and 69.72, respectively. The ratio of the observed Raman frequencies (~0.9) is close to the square root of the ratio of the atomic masses (~0.86), as would be expected for a vibrational mode in a similar potential involving essentially the Cr or the Ga atom. Comparing the INS response, we note a somewhat bigger difference, the peak seen at 5.5 meV in SGO appears at 7 meV in SGCO. Of course for modes with participation from many atomic species and different interatomic potentials, the simple comparison based on atomic mass only cannot be quantitatively correct.

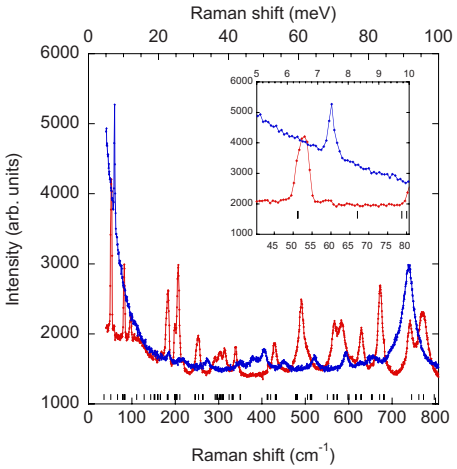

FIG. 2. (Color online) Raman spectra at $T=300$ K for SGO (red), with calculated Raman-active mode energies shown by the ticks at the bottom of the graph, and SCGO (blue, higher intensity at low energy). Both of these compounds have a Raman-active low-energy mode in the vicinity of the kink seen in the GDOS, compare with Fig. 3. The inset shows in detail the low-energy range highlighting the good match with the position calculated for SGO.

B. SGO/SCGO phonon response compared with calculation

Figure 4 compares the *ab initio* determined and measured GDOS for SGO. In order to compare with experimental data, the calculated GDOS was determined as the sum of the partial vibrational densities of states $g_i(\omega)$ weighted by the atomic scattering cross sections and masses: $\mathrm{GDOS}(\omega)=\Sigma_i(\sigma_i/M_i)g_i(\omega)$, where $[\sigma_i/M_i=0.265(\mathrm{O}),0.096(\mathrm{Ga}),0.071(\mathrm{Sr});i=(\mathrm{O},\mathrm{Ga},\mathrm{Sr})]$. A more detailed look at the neutron data on the SGO compound is shown in Fig. 5 where one can see that the low-energy phonon response is well described by a superposition

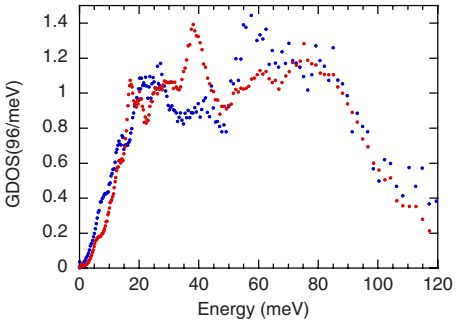

FIG. 3. (Color online) GDOS at $T=300$ K for SCGO (blue) and SGO (red), obtained using the data shown over a limited (Q,ω) range in Fig. 1. For SCGO, the weight of the paramagnetic contribution has been minimized using only the high-Q data ($Q_{el}>3.5$ Å^{-1}). Due to the remaining magnetic contribution in SCGO, the GDOS at low energy shows a faster Debye growth as compared to SGO. There are distinct differences in the phonon bands in the range $20<\hbar\omega<70$ meV but we can note a similar form at low energy, the peaked phonon response seen in SGO at $\hbar\omega\approx5.5$ meV and in SCGO at $\hbar\omega\approx7$ meV (see Fig. 1) produces a characteristic kink at that same position. A rather similar response of the two systems is observed in the high-energy range dominated by the oxygen modes.

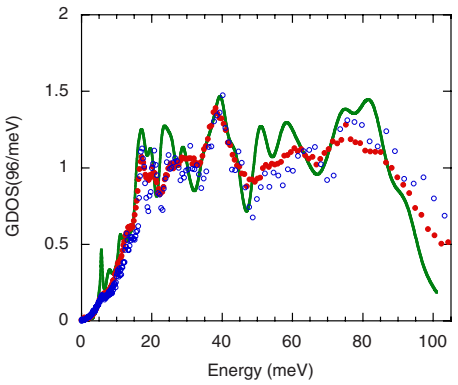

FIG. 4. (Color online) Calculated and neutron-determined GDOS for SGO show very similar overall features. The results using both IN4 (red dots) and IN6 (blue circles) data are in good agreement with the calculation (green solid line) and display a similar broadened peak at $\hbar\omega\approx5.5$ meV, see also Fig. 5. The calculated data has been convoluted with a Gaussian to account for the experimental resolution.

of a Debye term and a broadened peak at $\hbar\omega=5.5$ meV. The observed broadening of the peak $[\delta\approx2.3$ meV (FWHM)] does not depend on the instrumental resolution that is less than the apparent line width both on IN4 and on IN6. Disregarding the broadening, the calculated spectrum is in very good agreement with the observed one, in particular, the peak at ~5.5 meV is very well reproduced and also the relative weight of the peak is in reasonable agreement with calculation. The width of the peak is not resolution limited and we conclude that the mode seen in Raman spectrum reported in Fig. 2 is included in the peak of the GDOS. Due to the magnetic contribution present in SCGO fitting with the expected $\propto\omega^2$ and a Gaussian peak is not applicable. However, mimicking the magnetic contribution with an additional linear term, a reasonable fit can be obtained for the Gaussian

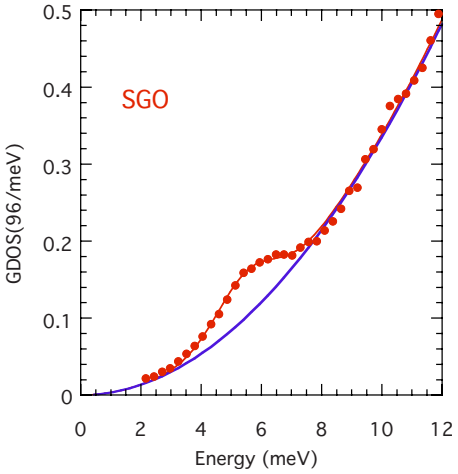

FIG. 5. (Color online) The low-energy part of the SGO-GDOS can be fitted (red line) with a superposition of a Debye term ($\propto\omega^2,\hbar\omega_D=46$ meV) (blue line) and single-mode peak with a Gaussian line shape. The results using both IN4 and IN6 (not shown) data are in good agreement and display a similar broadened peak at $\hbar\omega\approx5.5$ meV and $\delta=2.3$ meV (FWHM), indicating that this broadening is not due to instrumental resolution.

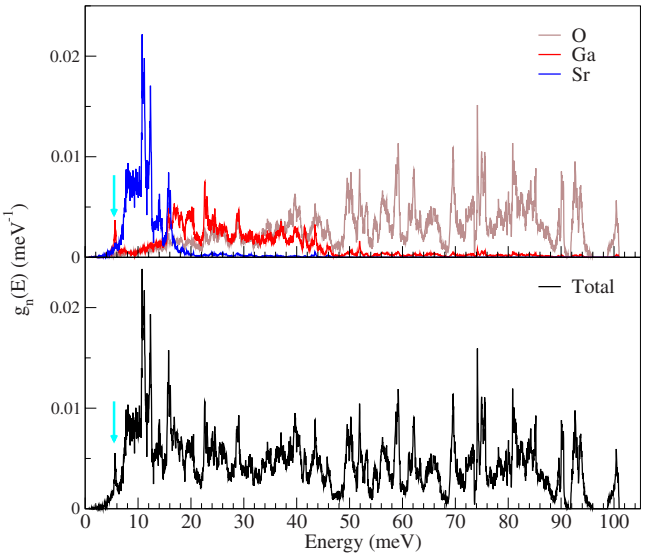

FIG. 6. (Color online) Calculated partial and total neutron-weighted GDOS for SGO. Arrows indicate the peak in the Ga partial corresponding to the phonon mode of interest at $\hbar\omega = 5.5$ meV.

peak at $\hbar\omega = 7$ meV with a width of $\delta \approx 2.4$ meV (FWHM) similar to the SGO case (not shown).

Based on the above, we can consider that the experimental data validates the computational approach in terms of the generalized density of states and Raman response. Accordingly, we can go further in analyzing the calculated partial GDOS. Figure 6 shows total (GDOS) and the partials $g_i(\omega)$ of SGO. The major contribution of the Ga atoms to the peaked low-energy response is clear. The Ga partial $g_{\mathrm{Ga}}(\omega)$ can be further resolved into the contributions from the different crystallographic sites $g_{\mathrm{Ga},j}(\omega)$, see Fig. 7. This is of interest for the case of SCGO since the magnetic Cr atoms

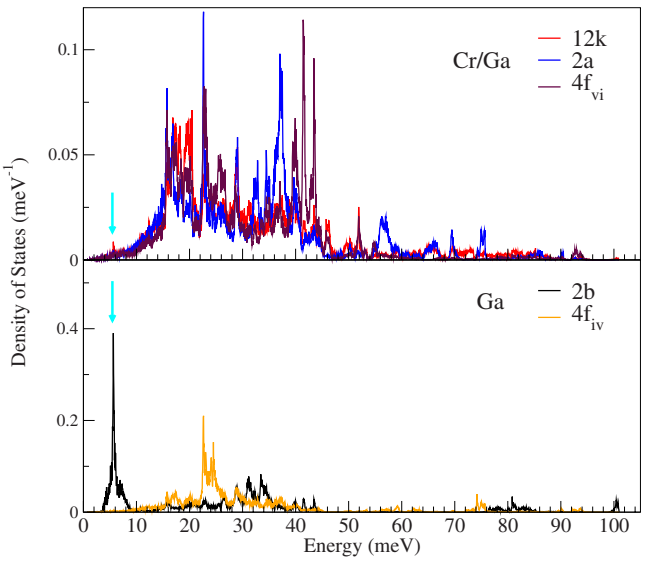

FIG. 7. (Color online) *Ab initio* determined partial DOS of Ga atoms, $g_{\mathrm{Ga},j}$, in SGO. The strongest contributions to the low-energy peak are from the $2b$ and $12k$ sites, respectively, as indicated by arrows. See Table I for details of site occupations.

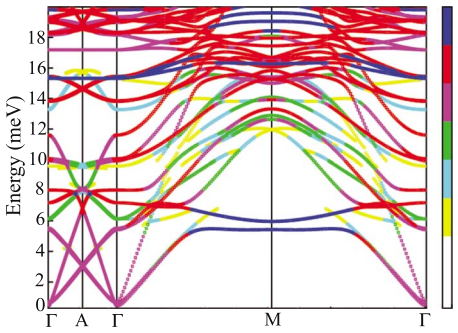

FIG. 8. (Color online) Calculated dispersion relations along the high-symmetry directions of the Brillouin zone in SGO, with color-coded neutron-scattering intensity, blue color corresponds to the maximum intensity. The Bradley-Cracknell notation is used for the high-symmetry points: $\Gamma=(0,0,0)$, $\mathrm{A}=(0,0,1/2)$, and $\mathrm{M}=(1/2,1/2,0)$.

occupy almost fully the sites $2a$, $12k$, and $4f_{vi}$ that contain only Ga in SGO, see Table I. It appears that the $2b$ and $12k$ site partials, $g_{\mathrm{Ga},2b}(\omega)$ and $g_{\mathrm{Ga},12k}(\omega)$ give the strongest contribution to the total density of states. The $2b$ site is fully occupied by the nonmagnetic Ga also in SCGO while the Cr occupation on the $12k$ and $2a$ sites, forming the pyrochlore slab, is beyond 90% in the least diluted samples[13] (see Table I and Fig. 10). Structural refinements of the isostructural magnetoplumbite compounds, including SGO,[26] usually indicate large Debye-Waller factor for the cation located in the trigonal bipyramid on the $2b$ site, and a split occupation on the $4e$ site can be considered (see Table I).

The high spectral weight of the $g_{\mathrm{Ga},2b}(\omega)$ partial is consistent with dynamical disorder being the reason for the large and anisotropic thermal displacement of Ga atom. The $12k$ and $2a$ sites constitute the pyrochlore slab magnetic sublattice, Kagome and triangular planes, respectively, in the SCGO compound, and we begin to understand how phonons at 7 meV can drive magnetic relaxation in SCGO.

Calculated phonon-dispersion relationships are shown in Fig. 8 in which the color-coded intensities correspond to the coherent, dynamic structure factor for one-phonon creation. Close to the GDOS low-energy peak (~6 meV), the dispersion curves consists of flat branches with two modes around the M point having maximal intensity. These modes make the strongest contribution to the DOS and we observe their signature in form of the Gaussian peak seen in the experimental GDOS. At the Γ point, there are three Raman-active modes close to the GDOS peak but with weaker response in the INS. Due to the fact that the nuclei of the SGO are coherent neutron scatterers, the inelastic-scattering cross section has characteristic features even in powder-averaged phonon response that can also be resolved in terms of its wave-vector dependence. In order to gain further confidence in the dispersion relations and the overall phonon response, we have calculated the coherent structure factor over the whole Brillouin zone. From this data, we have generated the $S(Q,\omega)$ map for a powder sample, using the recently developed, powder-averaged lattice-dynamics approach.[30,31] The calculated result can be compared with experimental data from IN4, see Fig. 9.

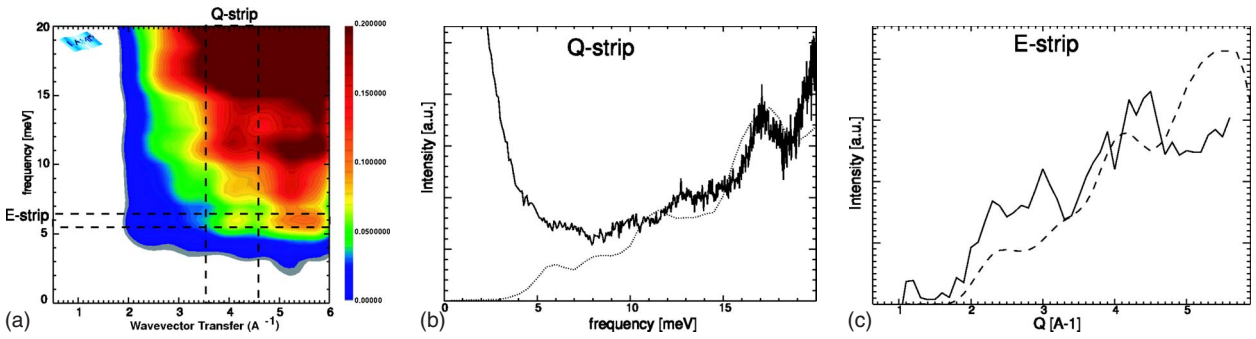

FIG. 9. (Color online) Simulated $S(Q,\omega)$ map (a) for SGO calculated for the Stokes (one-phonon annihilation) process at $T=0$, Fig. 1 shows the measured anti-Stokes (phonon-creation) response weighted by the thermal population. Therefore, the relative intensity at higher absolute value of energy transfer appears less in Fig. 1. Constant Q cut (b) of measured and calculated $S(Q,\omega)$ (solid and dotted lines, respectively). Constant energy cut (c) of measured and calculated $S(Q,\omega)$ (solid and dashed lines, respectively). The measured cuts shown here are the phonon-creation response ($\hbar\omega>0$) at $T=2$ K, note similarity of the constant energy cut (c) with the one shown in the lower right panel of Fig. 1 at $T=300$ K.

Comparison by eye of the low-energy spectrum is hampered by the elastic intensity in the experimental data, which is not calculated. Measured and calculated $S(Q,\omega)$ maps are, however, in reasonably good agreement as shown by constant energy and constant Q cuts.

One can also note that the modulations superposed on the overall Q^2 dependence of the inelastic signal at energy transfer of 5.5 meV appear periodically at positions close to the successive M-point values at $Q\approx 1.9$, 3.1, and 4.3 Å^{-1}. Note that the measured data shown in Fig. 9 is taken at low temperature, $T=2$ K, and therefore a shorter incident wavelength ($\lambda_i=1.8$ Å) was necessary, compared to the setting used to obtain the data shown in Fig. 1 ($\lambda_i=2.6$ Å), in order to reach high enough momentum transfer in the Stokes (neutron energy loss, phonon creation) side of the spectrum. The quality of the data at low temperature is worse due to reduced thermal population of phonon states. Also the energy resolution of the instrument is comparably worse. A check of the temperature dependence of the phonon response in SCGO in the vicinity of the spin-freezing transition did not indicate any significant change in the limits of experimental precision.

In view of the importance of the two M-point modes (5.6 and 6.2 meV), we show schematically their displacement vectors in Fig. 10 for the case of the SCGO magnetic compound. Therein the displacements of Cr and Ga atoms are highlighted. The sites 12*k* and 2*a* belong to the magnetically connected pyrochlore slab network, representing the triangular planes and the Kagome planes, respectively, and the vibrational characteristics, there should be the most important in the context of the magnetic relaxation. As depicted in Fig. 10, the M-point phonons involve large amplitude displacements of the Ga atoms on the 2*b* sites, and the associated response of the 2*a* and 12*k* sites will modulate the magnetic interactions between these sites. In this context, the observed phonon-driven magnetic relaxation could be explained as a consequence of the strong sensitivity of the magnetic interactions to subtle variations in the magnetic exchange pathways between adjacent Cr magnetic cations. It was shown that the antiferromagnetic coupling J between nearest-neighbor Cr ions within the pyrochlore slab is very sensitive to the Cr-Cr distance.[12] The J value follows a phenomenological law $\Delta J/\Delta d=450$ K/Å. Because phonon calculations could be done for SGO only, it is not possible however to give an accurate value for the J modulation associated with the M mode in SCGO.

C. Case of BSZGO/BSZGCO

We first examine the Raman response, Fig. 11. Here again we can see that both the magnetic and the nonmagnetic compounds display a low-energy Raman peak, reassembling the one observed in the SGO/SCGO systems. Also as before, one has a slightly lower energy for the peak in the Cr-containing compound, and this situation can be qualitatively ascribed to the difference in atomic mass. The experimental GDOS has a

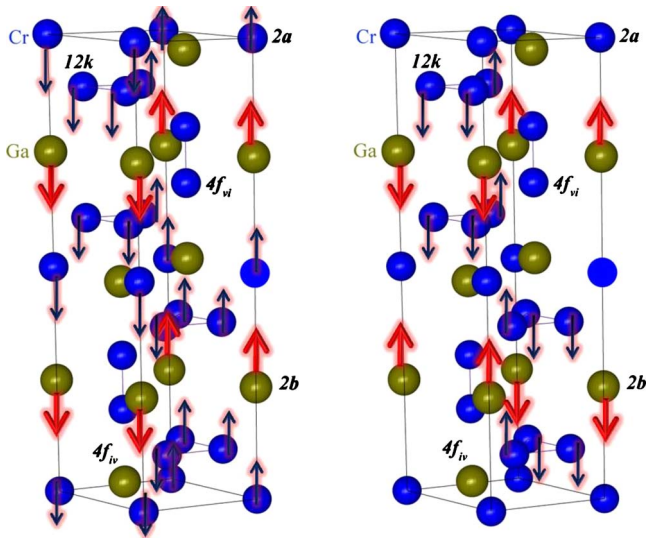

FIG. 10. (Color online) Schematic representations of the normal modes in SGO around the M point (1/2,1/2,0) at the zone boundary of the hexagonal Brillouin zone at $\hbar\omega=5.6$ meV (left) and at $\hbar\omega=6.2$ meV (right), with arrows indicating transverse cation displacements. The 2*a*, 12*k*, and $4f_{vi}$ are sites occupied in major part by Cr in SCGO. The 2*b* and $4f_{iv}$ are the sites occupied by Ga only both in SGO and in SCGO.

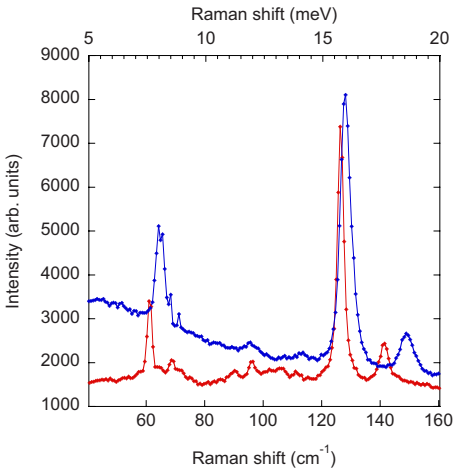

FIG. 11. (Color online) Raman spectra on BSZGO (red, lower) and BSZSCGO (blue, upper), measured at $T=300$ K. Note the low-energy mode similar to the SGO/SCGO case shown in Fig. 2.

dynamic range comparable to that of SGO/SCGO and especially the high-energy part shows similar form, Fig. 12. However, there is a qualitative difference in the experimental GDOS as compared with SGO, the one measured for BSZGO does not show any distinct peak in the range where the Raman peaks are visible. The low-energy phonon response is overall rather different, it does not show the characteristic ω^2 dependence typical of acoustic-phonon response associated with the Debye regime. In fact, we observe an almost linear dependence GDOS $\propto\omega$ with a progressive upward curvature that never reaches a quadratic law, see Fig. 13. Such a behavior is quite unusual. For crystalline solids, the acoustic phonons with linear dispersion should give a quadratic density of states. To explain the unconventional trend, we propose that the substitutional disorder in the form of 50/50 occupation by Zn or Ga on one of the $2d$ sites creates a situation that affects the lattice dynamics and gives rise to a disorder-induced dynamic response. We can argue that the damping of phonon modes due to the lattice disorder

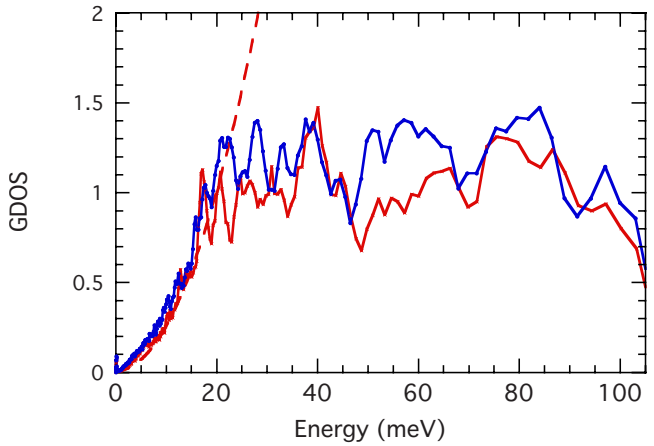

FIG. 12. (Color online) GDOS of BSZGO (blue) compared with that of SGO (red), normalized as explained in the text. For the latter note, the Debye-type dependence at low temperature (dashed line with $\hbar\omega_D=46$ meV), see also Fig. 5.

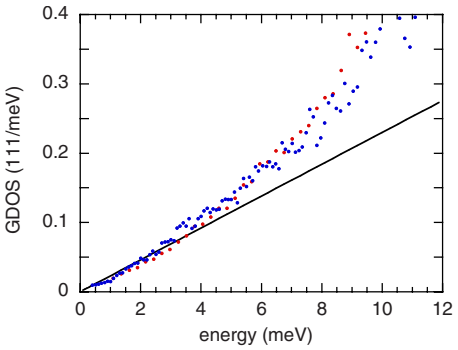

FIG. 13. (Color online) The low-energy part of the GDOS of BSZGO, the solid line showing the linear non-Debye dependence for $\hbar\omega\to 0$. Data with blue and red symbols from IN6 and IN4, respectively.

leads to the observed non-Debye response of the low-energy modes, not necessarily just the long-wavelength acoustic modes but also the ones further out in the Brillouin zone or even at the zone boundary.

V. DISCUSSION AND CONCLUSIONS

In the previous section, we have provided evidence of the possibility of particular normal modes being responsible for the magnetic relaxation in SCGO. We suggested that the activated behavior of the relaxation rate is due to the capacity of the phonons at that energy to influence the magnetic system. In the following, we attempt to examine more generally the role of phonons in the temperature dependence of the magnetic relaxation. We survey a possible minimal model in which the important issue is the capability of the phonon bath to provide energy for the magnetic system.

A. Magnetic relaxation controlled by phonon population

Let us assume that the phonon-dominated relaxation rate τ^{-1} is determined by the number of occupied phonon states, accordingly the temperature dependence is related to the thermal population $n_{ph}(T)$,

$$\tau(T)^{-1} \propto n_{ph}(T) = \int \frac{g(\omega)d\omega}{e^{\hbar\omega/k_BT}-1}. \tag{1}$$

In the case of a single mode of energy ω_m, we have $g(\omega)\propto\delta(\omega-\omega_m)$; and the phonon population and the relaxation rate have the activated dependence,

$$\tau^{-1} \propto n_{ph}(T) = \frac{1}{e^{\hbar\omega_m/k_BT}-1} \approx e^{-\hbar\omega_m/k_BT}, \tag{2}$$

where the approximation is valid at low temperatures when $\hbar\omega_m/k_BT \gg 1$. This dependence satisfies the experimental observation concerning the magnetic relaxation in SGCO. However, if any low-energy phonon can induce relaxation, one can expect that the low-energy density of states is the important quantity, and then the expected T dependence of the relaxation rate will depend on the functional form of the density of states $g(\omega)$. At low temperatures, the integration in

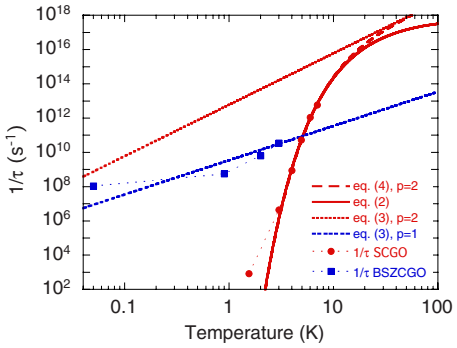

FIG. 14. (Color online) Modeling the relaxation, see details in the text. The single-frequency activated model of Eq. (2) follows the experimental data on SCGO over the range $3 \lesssim T \lesssim 7$ K as reported earlier (Ref. 11) and is in that temperature range indiscernible from the model with cutoff at the same frequency, Eq. (4). The trend of the power-law models Eq. (3) does not match the data points of neither SCGO (dots) nor BSZCGO (squares). Note that the two models have been plotted with arbitrarily chosen prefactors.

Eq. (1) can be taken from zero to infinity and after a transformation of variable $x=\hbar\omega/k_BT$, one finds that a power-law form $g(\omega) \propto \omega^p$ leads to a power law in T,

$$n_{ph}(T) \propto (k_BT/\hbar)^{p+1} \int_0^\infty \frac{x^p dx}{e^x - 1}, \tag{3}$$

where the definite integral can be evaluated analytically.[32] Another possible situation might be such that there is a low-energy cutoff ω_c due to, e.g., Q dependence of the effective interaction. In this case, for $\hbar\omega_c/k_BT \gg 1$, the number of phonons affecting the relaxation rate is evaluated to be

$$n_{ph}(T) \propto (k_BT/\hbar)^{p+1} \int_{\omega_c}^\infty \frac{x^p dx}{e^x} \propto (k_BT/\hbar)^{p+1} e^{-\hbar\omega_c/k_BT}. \tag{4}$$

We have seen above that the experimental GDOS is a superposition of the Debye ω^2 and a single-mode energy contribution in the case of SGO while in BSZGO, a linear ω dependence appears. In case of independent relaxation processes, one can expect that the relaxation rates of each process are additive,

$$\tau^{-1} = \sum_i \tau_i^{-1}. \tag{5}$$

It is straightforward to calculate $n_{ph}(T)$ in the Eqs. (1)–(4). Note, however, that to determine a quantitative estimate for the relaxation rate it would be necessary to know the prefactor describing the efficiency of the coupling between the spin system and the phonon bath. Experimentally, we find for the magnetic relaxation in SCGO that $\tau^{-1} = \tau_0^{-1} \exp(E_A/k_BT)$ with $\tau_0^{-1} = 7 \times 10^{17}$ s^{-1}. This means that a Debye phonon controlled relaxation of the type $\tau^{-1} = \tau_D^{-1} T^3$ would dominate at low temperatures for values of $\tau_D^{-1} \geq 10^{12}$ s^{-1}, see Fig. 14, which also shows that both the single mode and the cutoff picture could match equally well the experimental data on SCGO in the activated regime. It is not possible to discern any power-law dependence either for SCGO or BSZCGO suggesting that long-wavelength acoustic phonons are not effective for the magnetic relaxation process. We can also argue that both in SCGO and in BSZCGO at the lowest temperatures, a crossover to a quantum relaxation regime takes place,[11,15] and we know that at higher temperatures, a quasielastic response with a width proportional to temperature prevails.[33] Meanwhile, it is clear that the limited temperature range of the observations does not allow a full analysis of the relaxational dynamics. We suggest that the most effective modes are the ones in the vicinity of the M point of the reciprocal lattice, indeed these zone-boundary modes have a spatial structure on the scale of the in-plane lattice parameter, and therefore match the nearest-neighbor distance between the localized magnetic moments. With respect to the situation with BSZCGO, we have observed no specific activation energy and it is not possible to see any well-defined power-law dependence in the temperature dependence of the relaxation rate. We evoked earlier (Sec. IV C) the possibility of the disorder-induced modification of the lattice dynamics being the origin of the faster relaxation, due to heavily damped phonon modes. Note that here again the space scale is typical of the pyrochlore slab in-plane unit due to the half/half Zn/Ga substitutional disorder. It is conceivable that this disorder has a strong influence especially on the M-point zone-boundary modes that, in case of an overdamped response, can achieve a quasielastic character, and give rise to the linear GDOS as observed, as well as to the faster relaxation seen in BSZCGO. Anyhow, it is clear that the T^2 dependence that one might expect with reference to the model calculation is not observed.

B. Other aspects of the relaxation mechanism

Our results suggest an important role of lattice vibrations in the low-temperature spin dynamics of the frustrated magnets SCGO and BSZCGO. However, one cannot claim that spin-phonon coupling alone could be the origin of the complex relaxational behavior. The systems studied are disordered due to the nonmagnetic dilution that has been widely studied and is a known factor in the pyrochlore slab compounds.[12,13,34] It is even surprising that even though the phonon properties of the SGO/SCGO lattices appear somewhat better defined when compared to the BSZGO, it is in SCGO that very strongly stretched time decay occurs. A complete microscopic picture of the relaxation process is still to be constructed and one can imagine that the fine details of the magnetic states of lowest energy are of major importance in such a pursuit. Pursuing the analysis might be extremely difficult for systems such as the pyrochlore slabs but in simpler cases, details of spin-lattice coupling have been already examined and could pave the way for further work.[9,10] In the general context of frustrated magnetism, our results point out a trend that has been already evoked, the low-temperature and ground-state properties are highly sensitive to system-dependent perturbations. Nevertheless, the present work pinpoints the importance of lattice vibrations and their microscopic character in the control of the low-energy spin dynamics.

VI. SUMMARY

We have presented a detailed investigation of the phonon spectra in the pyrochlore slab compounds SCGO and

BSZCGO based on *ab initio* lattice-dynamics simulations, inelastic neutron-scattering, and Raman measurements, in order to investigate the origin and mechanisms of the recently observed[11] phonon-driven magnetic relaxation in SCGO. Since the magnetic signal dominates the neutron-scattering response at low-energy transfer, we have performed new experiments on the isostructural nonmagnetic material SGO. Moreover, the chemical disorder is difficult to include in the *ab initio* lattice-dynamics calculations so these have also focused on SGO. Results of the calculations for the GDOS and $S(Q,\omega)$ for SGO are in good agreement with the experimental data. Neutron and Raman experiments show the similarity of the phonon response in the magnetic system with respect to the nonmagnetic counterpart. The calculated partial density of states for SGO indicates that the strongest contribution to the total density of states stems from the vibrations of the Ga atoms on the 2*b* and 12*k* sites of the lattice, associated with flat dispersion branches centered at the zone-boundary M point in the *k* space. Thus, we conclude that the phonons response in SCGO corresponding to that at the M point in SGO comprises the partial contribution of the atoms residing on the 12*k* sites of the magnetic sublattice of SCGO. The most relevant M-point modes have displacement vectors that modulate the distances between Cr sites in the Kagome layers of the pyrochlore slab and therefore can effectively couple with the magnetic moments. The activation energy for magnetic relaxation is equal to the position of the characteristic peak in the experimental GDOS. Calculated energies of two of the Raman-active Γ-point modes are included in the energy range of this peak but they appear with less weight in the calculated GDOS.

In comparison BSZCGO, the other pyrochlore slab antiferromagnet shows a qualitatively different low-energy phonon response with an enhanced non-Debye low-energy response. We suggest that the faster relaxation without a particular energy scale is a consequence of this circumstance, which we attribute to the particular Ga/Zn disorder present in this compound. Future computational and theoretical work is called for to examine the interplay of magnetic interactions and the microscopic mechanisms associated with specific phonon displacements for better understanding of the reported phenomena.

ACKNOWLEDGMENT

C.P. thanks J. Y. Mevellec for the Raman measurements.

*Corresponding author; zbiri@ill.fr

[1] A. Ramirez, in *Handbook of Magnetic Materials*, edited by K. Buschow (Elsevier, Amsterdam, 2001), Vol. 13, p. 423.
[2] *Proceedings of the Highly Frustrated Magnetism 2003 Conference*, J. Phys.: Condens. Matter Vol. 16, edited by J. Stewart (Institute of Physics, Bristol, 2004).
[3] *Proceedings of the International Conference on Highly Frustrated Magnetism 2006*, 2J. Phys.: Condens. Matter Vol. 19, edited by Z. Hiroi and H. Tsunetsugu (Institute of Physics, Bristol, 2007).
[4] R. Moessner and A. Ramirez, Phys. Today **59**(2), 24 (2006).
[5] R. Moessner and J. T. Chalker, Phys. Rev. Lett. **80**, 2929 (1998).
[6] R. Moessner and J. T. Chalker, Phys. Rev. B **58**, 12049 (1998).
[7] R. Moessner, Can. J. Phys. **79**, 1283 (2001).
[8] O. Tchernyshyov, R. Moessner, and S. L. Sondhi, Phys. Rev. B **66**, 064403 (2002).
[9] A. B. Sushkov, O. Tchernyshyov, W. Ratcliff II, S. W. Cheong, and H. D. Drew, Phys. Rev. Lett. **94**, 137202 (2005).
[10] C. J. Fennie and K. M. Rabe, Phys. Rev. Lett. **96**, 205505 (2006).
[11] H. Mutka, G. Ehlers, C. Payen, D. Bono, J. R. Stewart, P. Fouquet, P. Mendels, J. Y. Mevellec, N. Blanchard, and G. Collin, Phys. Rev. Lett. **97**, 047203 (2006).
[12] L. Limot, P. Mendels, G. Collin, C. Mondelli, B. Ouladdiaf, H. Mutka, N. Blanchard, and M. Mekata, Phys. Rev. B **65**, 144447 (2002).
[13] C. Mondelli, H. Mutka, and C. Payen, Can. J. Phys. **79**, 1401 (2001).
[14] P. Bonnet, C. Payen, H. Mutka, M. Danot, P. Fabritchnyi, J. Stewart, A. Mellergård, and C. Ritter, J. Phys.: Condens. Matter **16**, S835 (2004).
[15] H. Mutka, C. Payen, G. Ehlers, J. R. Stewart, D. Bono, and P. Mendels, J. Phys.: Condens. Matter **19**, 145254 (2007).
[16] www.ill.eu
[17] H. Mutka, M. M. Koza, M. R. Johnson, Z. Hiroi, J.-I. Yamaura, and Y. Nagao, Phys. Rev. B **78**, 104307 (2008).
[18] www.cnrs-imn.fr
[19] P. E. Blöchl, Phys. Rev. B **50**, 17953 (1994).
[20] P. Hohenberg and W. Kohn, Phys. Rev. **136**, B864 (1964).
[21] W. Kohn and L. J. Sham, Phys. Rev. **140**, A1133 (1965).
[22] G. Kresse and J. Furthmüller, Comput. Mater. Sci. **6**, 15 (1996).
[23] G. Kresse and D. Joubert, Phys. Rev. B **59**, 1758 (1999).
[24] J. P. Perdew, K. Burke, and M. Ernzerhof, Phys. Rev. Lett. **77**, 3865 (1996).
[25] J. P. Perdew, K. Burke, and M. Ernzerhof, Phys. Rev. Lett. **78**, 1396 (1997).
[26] H. Graetsch and W. Gebert, Z. Kristallogr. **209**, 338 (1994).
[27] X. Obradors, A. Labarta, A. Isalgué, J. Tejada, J. Rodriguez, and M. Pernet, Solid State Commun. **65**, 189 (1988).
[28] K. Parlinski, Z.-Q. Li, and Y. Kawazoe, Phys. Rev. Lett. **78**, 4063 (1997).
[29] K. Parlinski, software PHONON, 2003.
[30] M. Johnson, M. Koza, L. Capogna, and H. Mutka, Nucl. Instrum. Methods Phys. Res. A **600**, 226 (2009).
[31] M. M. Koza, M. R. Johnson, R. Viennois, H. Mutka, L. Girard, and D. Ravot, Nature Mater. **7**, 805 (2008).
[32] J. Blundell and K. Blundell, *Concepts in Thermal Physics* (Oxford University Press, Oxford, New York, 2006).
[33] C. Mondelli, H. Mutka, C. Payen, B. Frick, and K. Andersen, Physica B **284-288**, 1371 (2000).
[34] D. Bono, L. Limot, P. Mendels, G. Collin, and N. Blanchard, Low Temp. Phys. **31**, 704 (2005).